

Electromagnetic Oscillations in a Spherical Conducting Cavity with Dielectric Layers. Application to Linear Accelerators

Władysław Żakowicz,^{1,*} Andrzej A. Skorupski,^{2,†} and Eryk Infeld^{2,‡}

¹*Institute of Physics, Polish Academy of Sciences, Al. Lotników 32/46, 02-668 Warsaw, Poland*

²*Department of Theoretical Physics, National Centre for Nuclear Research, Hoża 69, 00-681 Warsaw, Poland*

We present an analysis of electromagnetic oscillations in a spherical conducting cavity filled concentrically with either dielectric or vacuum layers. The fields are given analytically, and the resonant frequency is determined numerically. An important special case of a spherical conducting cavity with a smaller dielectric sphere at its center is treated in more detail. By numerically integrating the equations of motion we demonstrate that the transverse electric oscillations in such cavity can be used to accelerate strongly relativistic electrons. The electron's trajectory is assumed to be nearly tangential to the dielectric sphere. We demonstrate that the interaction of such electrons with the oscillating magnetic field deflects their trajectory from a straight line only slightly. The Q factor of such a resonator only depends on losses in the dielectric. For existing ultra low loss dielectrics, Q can be three orders of magnitude better than obtained in existing cylindrical cavities.

Keywords: Spherical Cavity, Spherical Dielectric Layer, TE Mode, TM Mode, Q Factor, Linear Accelerator

I. INTRODUCTION

It has been shown [1–3] that, if a plane electromagnetic wave is scattered on a finite dielectric object, structural resonances can be excited in the object (e.g., whispering gallery modes). They are associated with very high amplitudes of oscillating EM fields in the dielectric and its vicinity. Their maxima exceed values reached in resonant cavities of typical linear accelerators by several orders of magnitude. Therefore, one can think of applying these fields to accelerate charged particles [1–3]. Many other applications of the whispering gallery modes are described in [4–6].

As for the proposals given in [1–3], both light produced by lasers and microwaves are conceivable. However, it is difficult to achieve the required synchronization of wave particle in the optical frequency range. In the microwave frequency range, this mechanism would require excessive total excitation energy and so may not be practical.

In this paper we demonstrate that the last mentioned problem can be overcome by locating the dielectric object in a resonant cavity. This appeals to traditional accelerating structures used in SLAC, see **Figure 1**. In the latter case, maximum amplitudes of accelerating fields are restricted by Joule heating losses in conducting walls and electric breakdown. In this connection, in existing accelerators (e.g., in LHC) one avoids sharp edges of the walls and uses superconductive resonant cavities. Unfortunately, since superconductivity of the walls disappears if the magnetic field on the wall exceeds a critical value, the maximal values of accelerating fields in these highly complicated cavities are not much higher than those reached in SLAC.

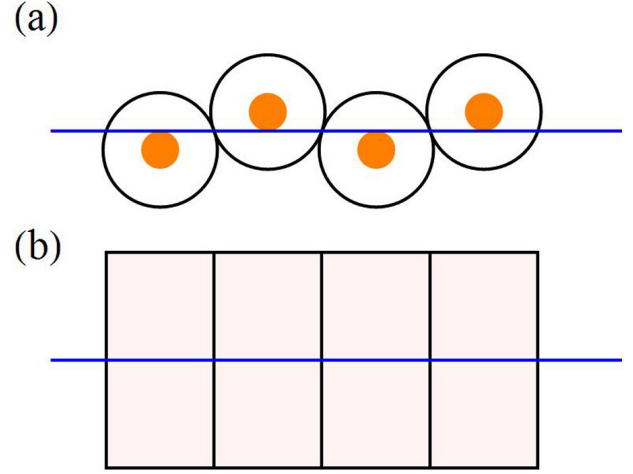


FIG. 1: Proposed multi cell accelerator units (a) vs. those of SLAC (b), assuming the same electron transit time through the cavity.

The presence of a dielectric in the central part of the resonance cavity shifts the magnetic field maximum from regions close to the metallic wall towards the dielectric surface. This considerably lowers skin effect losses in the wall. Even though additional losses due to dielectric heating are introduced, total losses would nevertheless be lower if one could apply ultra low loss dielectrics (with $\tan \delta \sim 10^{-7}$) as described in [7, 8]. In that case, a resonator quality reaching $Q \sim 10^7$ can be obtained, as compared to $Q \sim 10^4$ for SLAC.

II. A SPHERICAL CONDUCTIVE CAVITY WITH DIELECTRIC LAYERS

Our approach to describe electromagnetic oscillations in a resonant cavity assumes that the cavity can be di-

*wladyslaw.zakowicz@ifpan.edu.pl

†askor@fuw.edu.pl

‡infeld@fuw.edu.pl

vided into regions in which the fields can be determined analytically. The resonant frequency is defined by the fact that the fields must satisfy boundary conditions at the cavity wall along with continuity conditions at the interfaces. This frequency will be determined by numerically solving the consistency condition for these requirements.

In general, we assume that the cavity is bounded by a conducting spherical surface, and filled concentrically with N (≥ 1) either dielectric or vacuum layers. Each dielectric layer is assumed to be homogeneous. We introduce a spherical coordinate system (r, θ, ϕ) with its origin at the cavity center. The layers are bounded by $r = a_1, a_2, \dots, r_{N-1}$, up to $r = a_N \equiv b$ for the metallic boundary, see **Figure 2**.

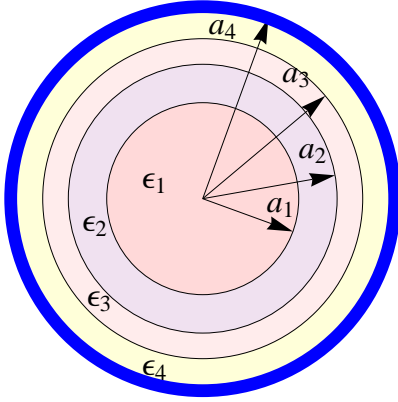


FIG. 2: An example of a spherical cavity with dielectric layers ($N = 4$).

The harmonically oscillating electromagnetic fields in each concentric layer are described by Maxwell's equations (Gaussian units, magnetic permeability $\mu = 1$, and complex fields proportional to $\exp(-i\omega t)$):

$$\nabla \times \mathbf{E} = ik\mathbf{B}, \quad \nabla \times \mathbf{B} = -ik\epsilon\mathbf{E} \quad (1)$$

where

$$k = \omega/c \quad (2)$$

ω is the angular frequency, and ϵ denotes complex dielectric permittivity

$$\epsilon = \epsilon' + i\epsilon'', \quad |\epsilon''| \ll \epsilon' \quad (3)$$

These fields split into transverse electric (TE) or transverse magnetic (TM), which have no radial components

of either field [9]. In an ideal resonator with perfectly conducting walls and perfect dielectrics, pure TE or TM modes can be excited. They will also be approximately valid in real resonators if their energy losses are not too high.

Using (9.116), and (9.119) in [9], which describe the vacuum TE field in spherical coordinates, and replacing there $k \rightarrow \sqrt{\epsilon}k$ we obtain the most general form of the TE field in the uniform dielectric:

$$\begin{aligned} \mathbf{E}^{lm}(\mathbf{r}, t) &= \mathbf{E}^{lm}(\mathbf{r}, \omega)e^{-i\omega t} \\ \mathbf{E}^{lm}(\mathbf{r}, \omega) &= \mathcal{E}_t(kr)\mathbf{X}^{lm}(\theta, \phi) \end{aligned} \quad (4)$$

where

$$\mathcal{E}_t(r) = A_l^{(1)}j_l(\sqrt{\epsilon}kr) + A_l^{(2)}y_l(\sqrt{\epsilon}kr) \quad (5)$$

$\mathbf{X}_{lm}(\theta, \phi)$ are vector spherical harmonics as defined by Eq. (9.119) in [9], and $j_l(\rho) \equiv \sqrt{\frac{\pi}{2\rho}}J_{l+\frac{1}{2}}(\rho)$ and $y_l(\rho) \equiv \sqrt{\frac{\pi}{2\rho}}Y_{l+\frac{1}{2}}(\rho)$ are spherical Bessel and Neumann functions.

The corresponding magnetic induction can be determined from the first Maxwell equation (1). Using also (10.60) in [9] we obtain

$$\mathbf{B} \equiv \mathbf{B}_{lm}(\mathbf{r}, t) = \mathbf{B}_{lm}(\mathbf{r}, \omega)e^{-i\omega t} \quad (6)$$

where $\mathbf{B}_{lm}(\mathbf{r}, \omega)$ involves both the transverse radial component:

$$\mathbf{B}_{lm}(\mathbf{r}, \omega) = \mathbf{B}_{lm\mathbf{t}}(\mathbf{r}, \omega) + \mathbf{B}_{lm\mathbf{r}}(\mathbf{r}, \omega) \quad (7)$$

in which

$$\mathbf{B}_{lm\mathbf{t}}(\mathbf{r}, \omega) = \mathcal{B}_t(r)\mathbf{n} \times \mathbf{X}_{lm}(\theta, \phi) \quad (8)$$

$$\mathbf{B}_{lm\mathbf{r}}(\mathbf{r}, \omega) = \mathcal{B}_r(r)Y_{lm}(\theta, \phi)\mathbf{n} \quad (9)$$

$$\mathcal{B}_t(r) = -\frac{i}{kr} \left[A_l^{(1)}j_l^D(\sqrt{\epsilon}kr) + A_l^{(2)}y_l^D(\sqrt{\epsilon}kr) \right] \quad (10)$$

$$\mathcal{B}_r(r) = \frac{\sqrt{l(l+1)}}{kr} \mathcal{E}_t(r) \quad (11)$$

Here $Y_{lm}(\theta, \phi)$ are spherical harmonics, $\mathbf{n} = \mathbf{r}/r$, l is a positive integer related to the integer m by $-l \leq m \leq l$, $j_l^D(\rho) \equiv \frac{d}{d\rho}(\rho j_l(\rho))$ and $y_l^D(\rho) \equiv \frac{d}{d\rho}(\rho y_l(\rho))$ are derivatives of the Riccati-Bessel and Riccati-Neumann functions.

In a similar way, using (9.118), (9.119) and (10.60) in [9] along with the second Maxwell equation (1), we obtain for the TM modes in the uniform dielectric:

$$\begin{aligned} \bar{\mathbf{B}}_{lm}(\mathbf{r}, t) &= \bar{\mathbf{B}}_{lm}(\mathbf{r}, \omega)e^{-i\omega t} \\ \bar{\mathbf{B}}_{lm}(\mathbf{r}, \omega) &= \bar{\mathcal{B}}_t(r)\mathbf{X}_{lm}(\theta, \phi) \end{aligned} \quad (12)$$

where

$$\bar{\mathcal{B}}_t(r) = \bar{A}_l^{(1)}j_l(\sqrt{\epsilon}kr) + \bar{A}_l^{(2)}y_l(\sqrt{\epsilon}kr) \quad (13)$$

$$\bar{\mathbf{E}} \equiv \bar{\mathbf{E}}_{lm}(\mathbf{r}, t) = \bar{\mathbf{E}}_{lm}(\mathbf{r}, \omega)e^{-i\omega t} \quad (14)$$

where $\bar{\mathbf{E}}_{lm}(\mathbf{r}, \omega)$ involves both the transverse, and radial component:

$$\bar{\mathbf{E}}_{lm}(\mathbf{r}, \omega) = \bar{\mathbf{E}}_{lm t}(\mathbf{r}, \omega) + \bar{\mathbf{E}}_{lm r}(\mathbf{r}, \omega) \quad (15)$$

in which

$$\bar{\mathbf{E}}_{lm t}(\mathbf{r}, \omega) = \bar{\mathcal{E}}_t(r) \mathbf{n} \times \mathbf{X}_{lm}(\theta, \phi) \quad (16)$$

$$\bar{\mathbf{E}}_{lm r}(\mathbf{r}, \omega) = \bar{\mathcal{E}}_r(r) Y_{lm}(\theta, \phi) \mathbf{n} \quad (17)$$

$$\bar{\mathcal{E}}_t(r) = \frac{i}{kr\epsilon} \left[\bar{A}_l^{(1)} j_l^D(\sqrt{\epsilon} kr) + \bar{A}_l^{(2)} y_l^D(\sqrt{\epsilon} kr) \right] \quad (18)$$

$$\bar{\mathcal{E}}_r(r) = -\frac{\sqrt{l(l+1)}}{kr\epsilon} \bar{\mathcal{B}}_t(r) \quad (19)$$

In our analysis we will admit small energy losses in both the wall and the dielectric layers. However, when calculating the resonant frequency of the cavity $\omega_0 \equiv \omega^l$, these losses will be neglected. Thus the wall is assumed to be perfectly conducting. This means that it carries no electric or magnetic field. Then continuity of the tangential components of the electric field and the normal components of the magnetic induction at each interface require vanishing of these components at the boundary of N th layer at $r = b$. In view of (4)–(9), and (12)–(19) this will be the case if the following boundary conditions at $r = b$ are fulfilled:

$$\begin{aligned} A_{lN}^{(1)} j_l(\sqrt{\epsilon_N} kb) + A_{lN}^{(2)} y_l(\sqrt{\epsilon_N} kb) &= 0 \\ \bar{A}_{lN}^{(1)} j_l^D(\sqrt{\epsilon_N} kb) + \bar{A}_{lN}^{(2)} y_l^D(\sqrt{\epsilon_N} kb) &= 0 \end{aligned} \quad (20)$$

where the upper line refers to TE modes and the lower one to TM modes.

In the first layer which contains the origin $r = 0$ we must choose

$$A_{l1}^{(2)} = 0 \quad \text{or} \quad \bar{A}_{l1}^{(2)} = 0 \quad (21)$$

to avoid singularities of $y_l(\rho)$ or $y_l^D(\rho)$ at $\rho = 0$.

In the simplest case of a spherical cavity filled completely with the dielectric (or vacuum), i.e., $N = 1$, the boundary conditions (20) lead to

$$j_l(\sqrt{\epsilon_1} kb) = 0 \quad \text{or} \quad j_l^D(\sqrt{\epsilon_1} kb) = 0 \quad (22)$$

where $\epsilon_1 \geq 1$, $k = \omega_0/c$. This defines the resonant frequency ω_0 of either TE or TM modes, depending only on $\epsilon_1 (= \epsilon_N)$ and b .

In the presence of layers ($N > 1$), ω_0 must also depend on ϵ_{N-1} , a_{N-1} etc. and therefore condition (22) cannot be fulfilled. In fact, for the same reason, we can assume that also the remaining functions in conditions (20) are non-vanishing. Therefore these conditions can be satisfied by choosing

$$A_{lN}^{(1)} = \frac{\mathcal{N}_l}{j_l(\sqrt{\epsilon_N} kb)}, \quad A_{lN}^{(2)} = -\frac{\mathcal{N}_l}{y_l(\sqrt{\epsilon_N} kb)} \quad (23)$$

$$\bar{A}_{lN}^{(1)} = \frac{\mathcal{N}_l}{j_l^D(\sqrt{\epsilon_N} kb)}, \quad \bar{A}_{lN}^{(2)} = -\frac{\mathcal{N}_l}{y_l^D(\sqrt{\epsilon_N} kb)} \quad (24)$$

for TE modes (upper line) or TM modes, where \mathcal{N}_l and $\bar{\mathcal{N}}_l$ are normalization factors.

At the interfaces between dielectrics, the following quantities must be continuous: the tangential components of the electric field and normal ones of the magnetic induction and furthermore, the tangential components of the magnetic induction, due to vanishing of the surface currents at the dielectric surface. For the TE modes, this leads to the following conditions at $r = a_n$, $n = 1, \dots, N-1$:

$$\begin{aligned} A_{ln}^{(1)} j_l(\rho_n) + A_{ln}^{(2)} y_l(\rho_n) &= A_{ln+1}^{(1)} j_l(\rho_n^+) + A_{ln+1}^{(2)} y_l(\rho_n^+) \\ A_{ln}^{(1)} j_l^D(\rho_n) + A_{ln}^{(2)} y_l^D(\rho_n) &= A_{ln+1}^{(1)} j_l^D(\rho_n^+) + A_{ln+1}^{(2)} y_l^D(\rho_n^+) \\ \rho_n &= \sqrt{\epsilon_n} k a_n \\ \rho_n^+ &= \sqrt{\epsilon_{n+1}} k a_n. \end{aligned} \quad (25)$$

This can be written in matrix form

$$\mathbf{M}_n \cdot \mathbf{A}_n = \mathbf{M}_n^+ \cdot \mathbf{A}_{n+1} \quad (26)$$

where

$$\begin{aligned} \mathbf{A}_n &= \begin{bmatrix} A_{ln}^{(1)} \\ A_{ln}^{(2)} \end{bmatrix} & \mathbf{M}_n &= \begin{bmatrix} j_l(\rho_n) & y_l(\rho_n) \\ j_l^D(\rho_n) & y_l^D(\rho_n) \end{bmatrix} \\ \mathbf{M}_n^+ &= \begin{bmatrix} j_l(\rho_n^+) & y_l(\rho_n^+) \\ j_l^D(\rho_n^+) & y_l^D(\rho_n^+) \end{bmatrix}. \end{aligned} \quad (27)$$

The \mathbf{M} matrices are non-singular:

$$\begin{vmatrix} j_l(\rho) & y_l(\rho) \\ j_l^D(\rho) & y_l^D(\rho) \end{vmatrix} = \frac{\pi}{2} \begin{vmatrix} J_{l+\frac{1}{2}}(\rho) & Y_{l+\frac{1}{2}}(\rho) \\ J'_{l+\frac{1}{2}}(\rho) & Y'_{l+\frac{1}{2}}(\rho) \end{vmatrix} = \frac{1}{\rho} \neq 0 \quad (28)$$

where last equality follows from the fact that $J_{l+\frac{1}{2}}(\rho)$ and $Y_{l+\frac{1}{2}}(\rho)$ are solutions of the Bessel equation

$$u''(\rho) + \frac{1}{\rho} u'(\rho) + \left[1 - \frac{(l+\frac{1}{2})^2}{\rho^2} \right] u(\rho) = 0.$$

Multiplying (26) by

$$\mathbf{M}_n^{-1} = \rho_n \begin{bmatrix} y_l^D(\rho_n) & -y_l(\rho_n) \\ -j_l^D(\rho_n) & j_l(\rho_n) \end{bmatrix} \quad (29)$$

we arrive at the recurrence relation

$$\mathbf{A}_n = \mathbf{M}_n^{-1} \cdot \mathbf{M}_n^+ \cdot \mathbf{A}_{n+1} \quad n = 1, \dots, N-1. \quad (30)$$

For the n th interface between dielectrics, this relation defines the vector \mathbf{A} at the lower layer in terms of that at the upper one. Using this relation successively for $n = N-1, N-2, \dots, 1$, we can express all \mathbf{A}_n vectors in terms of

$$\mathbf{A}_N = \mathcal{N}_l \begin{bmatrix} 1 \\ \frac{j_l(\rho_N)}{1} \\ -\frac{1}{y_l(\rho_N)} \end{bmatrix} \equiv \mathcal{N}_l \mathbf{a}_N \quad \rho_N = \sqrt{\epsilon_N} kb \quad (31)$$

i.e.,

$$\mathbf{A}_n = (\mathbf{M}_n^{-1} \cdot \mathbf{M}_n^+) \cdot (\mathbf{M}_{n+1}^{-1} \cdot \mathbf{M}_{n+1}^+) \cdots (\mathbf{M}_{N-1}^{-1} \cdot \mathbf{M}_{N-1}^+) \cdot \mathbf{A}_N \equiv \mathcal{N}_l \mathbf{a}_n. \quad (32)$$

We recall that in the first layer we must satisfy $A_{l1}^{(2)} = 0$, see (21). In view of this requirement, equations (25) for $n = 1$ can be written as

$$\begin{aligned} A_{l1}^{(1)} j_l(\rho_1) - \mathcal{N}_l \left[a_2^{(1)} j_l(\rho_1^+) + a_2^{(2)} y_l(\rho_1^+) \right] &= 0 \\ A_{l1}^{(1)} j_l^D(\rho_1) - \mathcal{N}_l \left[a_2^{(1)} j_l^D(\rho_1^+) + a_2^{(2)} y_l^D(\rho_1^+) \right] &= 0 \end{aligned} \quad (33)$$

where $\rho_1 = \sqrt{\epsilon_1} k a_1$, $\rho_1^+ = \sqrt{\epsilon_2} k a_1$, and $a_2^{(1,2)}$ are components of the vector $\mathbf{a}_2 \equiv \mathbf{A}_2 / \mathcal{N}_l$. This vector is defined by (32) and (31) if $N > 2$ ($\rho_N = \sqrt{\epsilon_N} k b$):

$$\mathbf{a}_2 = (\mathbf{M}_2^{-1} \cdot \mathbf{M}_2^+) \cdot (\mathbf{M}_3^{-1} \cdot \mathbf{M}_3^+) \cdots (\mathbf{M}_{N-1}^{-1} \cdot \mathbf{M}_{N-1}^+) \cdot \begin{bmatrix} 1 \\ j_l(\rho_N) \\ 1 \\ -y_l(\rho_N) \end{bmatrix}. \quad (34)$$

For $N = 2$, \mathbf{a}_2 is defined by (31), i.e., is given by the last factor in (34).

The linear and homogeneous set of equations (33) for $A_{l1}^{(1)}$ and \mathcal{N}_l will have non-zero solutions if and only if its determinant vanishes,

$$\begin{aligned} j_l(\rho_1) \left[a_2^{(1)} j_l^D(\rho_1^+) + a_2^{(2)} y_l^D(\rho_1^+) \right] \\ - j_l^D(\rho_1) \left[a_2^{(1)} j_l(\rho_1^+) + a_2^{(2)} y_l(\rho_1^+) \right] &= 0. \end{aligned} \quad (35)$$

If this condition is fulfilled, $A_{l1}^{(1)}$ is given by either of equations (33), which are equivalent. Like all remaining coefficients $A_{ln}^{(1)}$ and $A_{ln}^{(2)}$, $n = 2, \dots, N$, also $A_{l1}^{(1)}$ will be proportional to the normalization factor \mathcal{N}_l , see (32) and (33).

If there are only two layers ($N = 2$), $a_2^{(1)}$ and $a_2^{(2)}$ in (33) and (35) are given by (31) and the resonant frequency ω_0 defined by (35) can be found from

$$\begin{aligned} j_l(\sqrt{\epsilon_1} k a_1) \left[\frac{j_l^D(\sqrt{\epsilon_2} k a_1)}{j_l(\sqrt{\epsilon_2} k b)} - \frac{y_l^D(\sqrt{\epsilon_2} k a_1)}{y_l(\sqrt{\epsilon_2} k b)} \right] \\ - j_l^D(\sqrt{\epsilon_1} k a_1) \left[\frac{j_l(\sqrt{\epsilon_2} k a_1)}{j_l(\sqrt{\epsilon_2} k b)} - \frac{y_l(\sqrt{\epsilon_2} k a_1)}{y_l(\sqrt{\epsilon_2} k b)} \right] &= 0. \end{aligned} \quad (36)$$

and

$$A_{l1}^{(1)} = \mathcal{N}_l \frac{1}{j_l(\sqrt{\epsilon_1} k a_1)} \left[\frac{j_l(\sqrt{\epsilon_2} k a_1)}{j_l(\sqrt{\epsilon_2} k b)} - \frac{y_l(\sqrt{\epsilon_2} k a_1)}{y_l(\sqrt{\epsilon_2} k b)} \right]. \quad (37)$$

By replacing in (25)–(37)

$$\begin{aligned} A_{lm}^{(1,2)} &\rightarrow \bar{A}_{lm}^{(1,2)}, \quad j_l^D(\sqrt{\epsilon_m} k a) \rightarrow j_l^D(\sqrt{\epsilon_m} k a) / \epsilon_m, \\ y_l^D(\sqrt{\epsilon_m} k a) &\rightarrow y_l^D(\sqrt{\epsilon_m} k a) / \epsilon_m \end{aligned} \quad (38)$$

for any m and a , we obtain the corresponding equations for the TM modes.

Any standard software like *Mathematica* or *Maple* can be used to solve the non-linear equation (35) or (36) defining the resonant frequency $\omega_0 \equiv \omega^l$, along with the pertinent linear algebra for $N > 2$. We did it for $N = 2$, see the following section, and also for $N = 3$, by using *Mathematica*.

Note that for the TM modes, where $\bar{\mathcal{B}}_t(r)$ in (19) is continuous at each dielectric interface, $\bar{\mathcal{E}}_r(r)$ will have jumps, due to discontinuities in ϵ . However, the radial component of the electric displacement $\bar{\mathcal{D}}_r(r) \equiv \epsilon \bar{\mathcal{E}}_r(r)$ will be continuous. This will also be true of the TE modes where the radial displacement is identically zero. These facts imply the vanishing of surface charges at each dielectric interface. And this in turn means that the multi-layer dielectric structure resembles (and can approximate) a smooth dielectric with some permittivity profile $\epsilon(r)$, in spite of jumps in ϵ .

It was pointed out to us by Paul Martin of SIAM, that our matrix equation (26), which can be used to relate the EM fields of a given mode for two layers of a stratified sphere, is not new. It was probably first used by A. Moroz [10] when calculating forced oscillations in such a sphere but without a conducting wall, induced by an oscillating electric dipole. In this application, the frequency ω is arbitrary.

III. A SPHERICAL CONDUCTIVE CAVITY WITH A DIELECTRIC SPHERE

The general theory given in the previous section will now be illustrated by calculations pertinent to the TE modes in a spherical cavity with a dielectric sphere of radius a and dielectric permittivity ϵ , i.e., for $N = 2$, $a_1 \equiv a$, $\epsilon_1 \equiv \epsilon$, and $\epsilon_2 = 1$.

Fields in such a system will be described by equations (4) – (9) both in the sphere and the surrounding vacuum. In view of (21) and (23) their radial profiles will be given by

$$\mathcal{E}_t(r) = \mathcal{N}_l \times \begin{cases} \mathcal{A}_l j_l(\sqrt{\epsilon} k r) & \text{if } 0 \leq r \leq a \\ \frac{j_l(kr)}{j_l(kb)} - \frac{y_l(kr)}{y_l(kb)} & \text{if } a \leq r \leq b \end{cases} \quad (39)$$

$$\mathcal{B}_t(r) = -\frac{i \mathcal{N}_l}{kr} \times \begin{cases} \mathcal{A}_l j_l^D(\sqrt{\epsilon} k r) & \text{if } 0 \leq r \leq a \\ \frac{j_l^D(kr)}{j_l(kb)} - \frac{y_l^D(kr)}{y_l(kb)} & \text{if } a \leq r \leq b. \end{cases} \quad (40)$$

Replacing $\epsilon_1 \rightarrow \epsilon$, $\epsilon_2 \rightarrow 1$ and $A_{l1}^{(1)} \rightarrow \mathcal{A}_l$ in (36) and (37), we obtain equations defining the resonant frequency ω^l and the amplitude coefficient \mathcal{A}_l .

We verified that for $\omega = \omega^l$, the average energies associated with the electric and the magnetic field in the

cavity are equal:

$$\begin{aligned} & \int_V \epsilon' |\mathbf{E}_{lm}(\mathbf{r}, \omega^l)|^2 dv \\ &= \int_V (|\mathbf{B}_{lm t}(\mathbf{r}, \omega^l)|^2 + |\mathbf{B}_{lm r}(\mathbf{r}, \omega^l)|^2) dv. \end{aligned} \quad (41)$$

(This was a check on the correctness of our formulas and accuracy of calculations.) The normalization constant \mathcal{N}_l was chosen so as to satisfy:

$$\begin{aligned} & \frac{1}{2} \left(\int_0^a \epsilon' |\mathcal{E}_t(r)|^2 r^2 dr + \int_a^b |\mathcal{E}_t(r)|^2 r^2 dr \right. \\ & \left. + \int_0^b (|\mathcal{B}_t(r)|^2 + |\mathcal{B}_r(r)|^2) r^2 dr \right) = 1. \end{aligned} \quad (42)$$

(The corresponding average energy associated with the electric and the magnetic field over our cavity is $1/(8\pi)$ erg.)

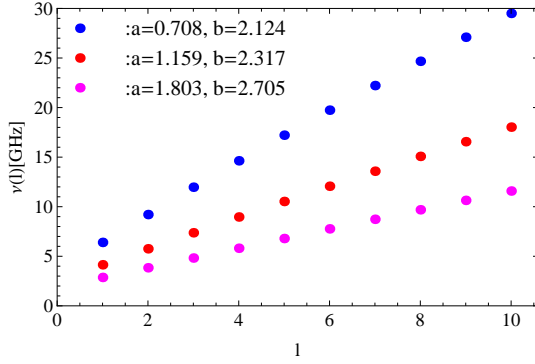


FIG. 3: The resonant frequencies $\nu(l) = \omega^l/(2\pi)$ versus l for three spherical cavities with dielectric spheres (a and b in cm). Note that ν is m independent (due to degeneracy).

In **Figure 3**, $\nu(l) = \omega^l/(2\pi)$ as a function of l is presented for three spherical cavities with dielectric spheres. Note that ν is m independent (due to degeneracy). This fact is one of the reasons why the spherical resonator shown in **Figure 1** cannot be used in the final project of a real accelerator even though it is very convenient for a general analysis. The degeneration in question can be broken e.g., by replacing the spherical resonator by an ellipsoidal one, or shifting the center of the dielectric sphere. In any case, however, a separate numerical analysis would be necessary.

In **Figure 4** we give an example of radial functions in the equations describing fields in our spherical cavity with a dielectric sphere, (4), (8) and (9). Large values of these functions in a vicinity of the dielectric boundary can be observed.

A. The motion of relativistic electrons

The trajectory $\mathbf{r}(t)$ of a relativistic electron crossing the spherical cavity shown in **Figure 1** can be

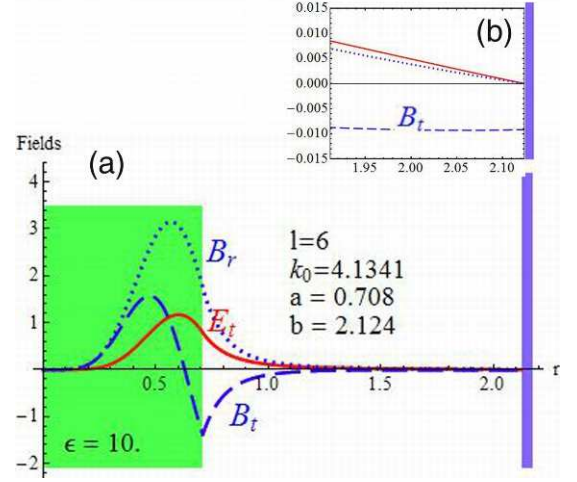


FIG. 4: (a) Field radial functions for a spherical cavity with dielectric sphere and perfect metallic wall (Gaussian units, $k_0 = \omega^l/c$, a and b in cm). The complete fields are given by (4) – (11). Note that \mathcal{E}_t and \mathcal{B}_r vanish at the wall, whereas \mathcal{B}_t is non-zero but small, see (b).

parametrized by the electron's closest approach $\mathbf{r}_0 = \mathbf{r}(t_0)$ and electron velocity $c\vec{\beta}$, $|\vec{\beta}| = 1$:

$$\mathbf{r}(t) = \mathbf{r}_0 + c\vec{\beta}(t - t_0). \quad (43)$$

The origin of the Cartesian coordinate system (x, y, z) was chosen at the center of the dielectric sphere, and the electron moving along the x axis was passing just above the dielectric sphere as shown in **Figure 1**. We chose

$$\mathbf{r}_0 = 1.01a(0, \sin \theta_0, \cos \theta_0), \quad \vec{\beta} = (1, 0, 0). \quad (44)$$

The effective accelerating field felt by the electron as it passes through the cavity, E_{eff} , is equal to the real part of $(c dt = dx)$

$$\bar{E}(l, m, \theta) \equiv |\bar{E}|e^{i\varphi} = \frac{c}{d} \int_{t_0 - \frac{d}{2c}}^{t_0 + \frac{d}{2c}} E_x(\mathbf{r}(t), \omega^l) e^{-i\omega^l t} dt, \quad (45)$$

where $d = 2\sqrt{b^2 - (1.01a)^2}$ is the electron trajectory segment within the cavity, E_x is the x component of the electric field $\mathbf{E}^{lm}(\mathbf{r}, \omega^l)$ given by (4) and $\mathbf{r}(t)$ is given by (43). Thus

$$E_{\text{eff}} = |\bar{E}| \cos \varphi, \quad \varphi = f(l, m, \theta) - \omega^l t_0. \quad (46)$$

Maximal acceleration is obtained ($E_{\text{eff}} = |\bar{E}|$) if t_0 is chosen so that the accelerating phase $\varphi = 0$. With this choice, the relativistic electron is never decelerated within the spherical cavity, see **Figure 7**, where two examples are given. Typical results for $E_{\text{eff}}|_{\varphi=0}$ obtained with our normalization (42) are shown in **Figures 5** and **6**.

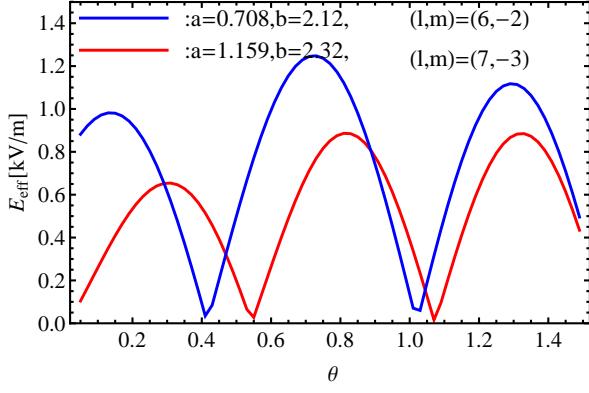


FIG. 5: Effective accelerating field as a function of θ_0 for two spherical cavities (a and b in cm).

The electromagnetic field given by the real parts of (4), (8) and (9) is strongly non-uniform. Therefore one should check how much the relativistic electron will deflect from the assumed trajectory $\mathbf{r}(t)$ given by (43), due to interaction with this field. A nice feature of our model is that the field in question is described analytically by (4)–(9) so that the pertinent equations of the transversal motion can easily be integrated numerically.

In a real accelerator, where we are dealing with an electron beam of finite cross section, the electromagnetic fields $\mathbf{E}(\mathbf{r}(t), t)$ and $\mathbf{B}(\mathbf{r}(t), t)$ acting on each electron will be superpositions of the external fields and the fields due to the electron charge and current. However, in the lowest approximation (and particularly for not too large beam densities) the latter fields can be neglected. Furthermore, if as in our case, the transversal deflections are small, the deflecting fields can be calculated on the unperturbed trajectory given by (43). It will also be assumed that the electron mass $m_e = m_{e0} \gamma$, $\gamma \gg 1$, is time independent within the spherical cavity. With these approximations, and within the Cartesian coordi-

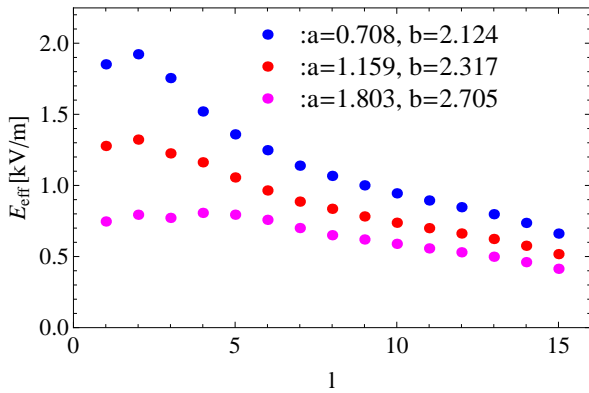


FIG. 6: Effective accelerating fields versus l for three spherical cavities with the assumed normalization of the RF field, see (42) (a and b in cm). For each value of l , these values were optimized with respect to m as well as θ_0 , see **Figure 5**.

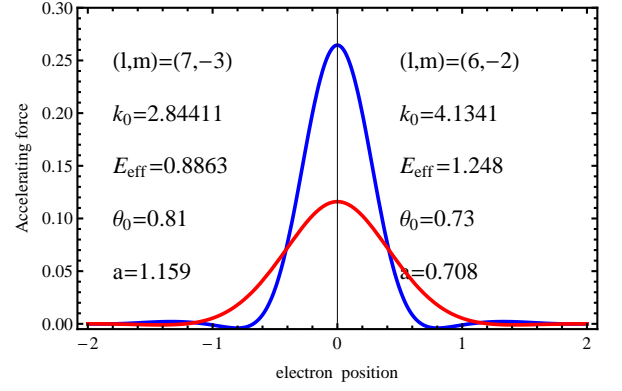


FIG. 7: The accelerating force (in units of 4.8032×10^{-10} dyne) acting on an electron as it moves through the cavity shown in **Figure 1** ($k_0 = \omega^l/c$, E_{eff} in kV/m, and dimensions in cm).

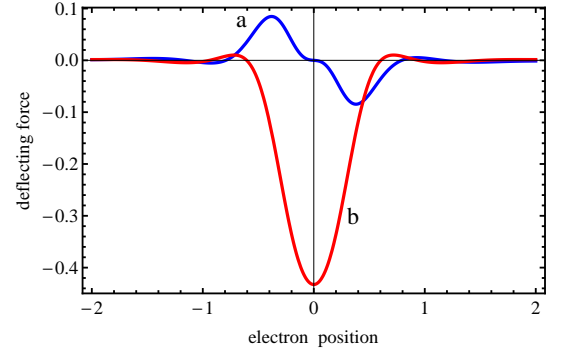


FIG. 8: The deflecting force coordinate $F_{\bar{y}}(\bar{x})$ for the accelerating phase $\varphi = 0$ (a) and $\varphi = \pi/2$ (b), see **Figure 7** for units and parameters (right column).

nate system $(\bar{x}, \bar{y}, \bar{z})$ with its center at \mathbf{r}_0 , the \bar{x} axis along the unperturbed trajectory, and the \bar{y} axis along \mathbf{r}_0 , the electron's transversal motion will be described by

$$m_e \frac{dv_{\bar{y}}}{dt} = -e[E_{\bar{y}} - B_{\bar{z}}], \quad v_{\bar{y}} = \frac{d\bar{y}}{dt} \quad (47)$$

$$m_e \frac{dv_{\bar{z}}}{dt} = -e[E_{\bar{z}} + B_{\bar{y}}], \quad v_{\bar{z}} = \frac{d\bar{z}}{dt} \quad (48)$$

where $\bar{t} = t - t_0$, the field components $E_{\bar{y}}(\bar{x}, \bar{t})$, $B_{\bar{z}}(\bar{x}, \bar{t})$, etc. are given by the real parts of Eqs. (4), (8) and (9), taken at $\bar{x} = c\bar{t}$, and $\bar{y} = \bar{z} = 0$. Integrating these equations with zero initial conditions we end up with ($d\bar{x} = c d\bar{t}$)

$$v_{\bar{y}}(\bar{x}) = -\frac{e}{m_e c} \int_{-d/2}^{\bar{x}} F_{\bar{y}}(\bar{x}') d\bar{x}' \quad (49)$$

$$v_{\bar{z}}(\bar{x}) = -\frac{e}{m_e c} \int_{-d/2}^{\bar{x}} F_{\bar{z}}(\bar{x}') d\bar{x}' \quad (50)$$

$$\bar{y}(\bar{x}) = \frac{1}{c} \int_{-d/2}^{\bar{x}} v_{\bar{y}} d\bar{x}', \quad \bar{z}(\bar{x}) = \frac{1}{c} \int_{-d/2}^{\bar{x}} v_{\bar{z}} d\bar{x}' \quad (51)$$

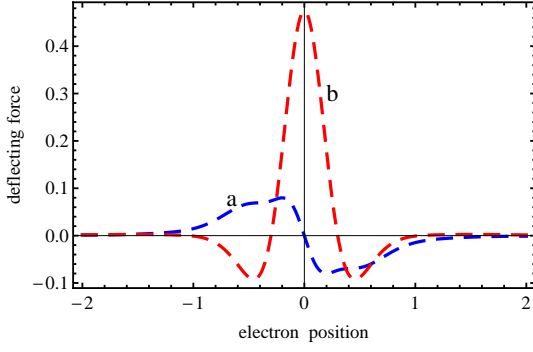


FIG. 9: The deflecting force coordinate $F_z(\bar{x})$ for the accelerating phase $\varphi = 0$ (a) and $\varphi = \pi/2$ (b), see **Figure 7** for units and parameters (right column).

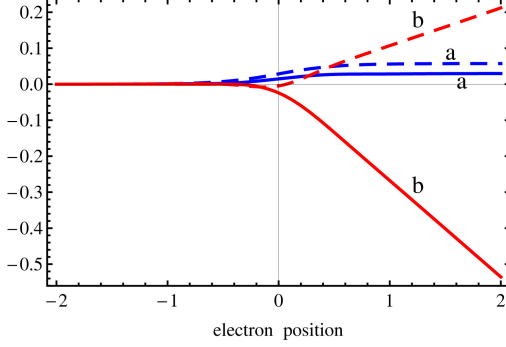


FIG. 10: Conveniently normalized transversal displacements \bar{y} (solid curves) and \bar{z} (dashed curves) as functions of \bar{x} for the accelerating phase $\varphi = 0$ (a) and $\varphi = \pi/2$ (b), see **Figure 7** for units and parameters (right column).

where $F_{\bar{y}} = E_{\bar{y}} - B_{\bar{z}}$, and $F_{\bar{z}} = E_{\bar{z}} + B_{\bar{y}}$.

In **Figures 8** and **9** we give an example of the coordinates $F_{\bar{y}}(\bar{x})$ and $F_{\bar{z}}(\bar{x})$ of the deflecting force. They correspond to $a = 0.708$ cm, $b = 2.124$ cm, and $(l, m) = (6, -2)$, for which the the accelerating field will be our reference value

$$E_{\text{eff}} \Big|_{\varphi=0} \equiv E_{\text{eff ref}} = 1.2366 \text{ kV/m}. \quad (52)$$

It can be seen that if the accelerating phase $\varphi = 0$, both $F_{\bar{y}}(\bar{x})$ and $F_{\bar{z}}(\bar{x})$ are odd functions. Therefore in this case of maximal acceleration, there will be no transversal velocity increments over the cavity, $v_{\bar{y}}(d/2) = v_{\bar{z}}(d/2) = 0$. At the same time the velocity components $v_{\bar{y}}(\bar{x})$ and $v_{\bar{z}}(\bar{x})$ in (51) will be even functions of \bar{x} tending to zero as $\bar{x} \rightarrow d/2$. Hence the transversal deflections $\bar{y}(\bar{x})$ and $\bar{z}(\bar{x})$ will be increasing functions tending to constants as $\bar{x} \rightarrow d/2$, see **Figure 10(a)**.

For the worst case of accelerating phase ($\varphi = \pi/2$) for which $E_{\text{eff}} = 0$, $v_{\bar{y}}(\bar{x})$ and $v_{\bar{z}}(\bar{x})$ will be increasing functions soon reaching their limiting values $v_{\bar{y}}(d/2)$ and $v_{\bar{z}}(d/2)$ for $\bar{x} > 0$. The corresponding transversal motions $\bar{y}(\bar{x})$ and $\bar{z}(\bar{x})$ will soon become uniform for $\bar{x} > 0$, leading to much larger deflections at $\bar{x} = d/2$, see **Figure 10(b)**.

The actual transversal deflections per cavity in an accelerator involving our spherical cavities can be obtained by multiplying the normalized values given in **Figure 10** by the factor

$$\alpha = \frac{e}{m_e} \frac{E_{\text{eff}}}{E_{\text{eff ref}}} \text{ cm} = 5.9 \times 10^{-4} \frac{E_{\text{eff}}/E_{\text{eff ref}}}{\gamma} \text{ cm} \quad (53)$$

where $E_{\text{eff ref}}$ is given by (52), E_{eff} is the assumed value of the effective accelerating field, and $\gamma = m_e/m_{e0}$. For large values of E_{eff} , small α requires γ to be sufficiently large. Assuming that $\bar{z}_{\text{max}} (= \bar{z}(d/2) > \bar{y}(d/2))$, see **Figure 10 (a)** is not larger than $p\%$ of the spacing between the dielectric sphere and the electron trajectory, $0.01a$, $a = 0.708$ cm, the required minimal electron energy is given by

$$m_e c^2 [\text{GeV}] = \frac{20.69}{p} \frac{E_{\text{eff}} [\text{MV/m}]}{100}. \quad (54)$$

Thus, if we assume that $E_{\text{eff}} = 100$ MV/m, the transversal displacements will be smaller than 1% of the spacing in question, if the electron energy $m_e c^2 \geq 21$ GeV, i.e., for typical output energies from SLAC. Whether the real dielectric can withstand this value of E_{eff} is another question beyond the scope of this paper. More comments will be given later on.

B. Quality factors

An important parameter of any linear accelerator is the quality Q of its resonant cavities:

$$Q = \omega_0 \frac{U}{P} \equiv 2\pi \frac{U}{T_0 P} \quad (55)$$

where ω_0 is the resonant angular frequency of the ideal cavity ($\sigma = \infty, \epsilon'' = 0$), T_0 is the corresponding resonant period, U is the time-averaged energy stored in the cavity ($\mu = 1$)

$$U = \frac{1}{16\pi} \int_V (\epsilon' |\mathbf{E}|^2 + |\mathbf{H}|^2) dv \quad (56)$$

and P is time-averaged cavity power loss.

The power loss caused by the skin current in the metallic wall bounded by the surface S is given by

$$P_{\text{met}} = \alpha \int_S |\mathbf{H}|^2 ds \quad (57)$$

where

$$\alpha = \frac{c}{8(2\pi)^{3/2}} \sqrt{\frac{\omega_0}{\sigma}} \equiv \frac{c^2}{32\pi^2 \sigma \delta}, \quad \delta = \frac{c}{\sqrt{2\pi\sigma\omega_0}} \quad (58)$$

δ is the skin depth, σ is conductivity of the wall, and the magnetic field intensity \mathbf{H} refers to the ideal cavity, i.e., its normal component is vanishing ($\mathbf{H} = \mathbf{H}_t$).

The quality of the cavity related to losses in the metallic wall is thus given by

$$Q_{\text{met}} = \omega_0 \frac{U}{P_{\text{met}}}. \quad (59)$$

Using the fact that at resonance, the averaged energies stored in the electric and magnetic fields are equal, see (41), we end up with ($\mathbf{H} = \mathbf{B}$):

$$Q_{\text{met}} = \frac{2}{\delta} \frac{\int_V |\mathbf{B}|^2 dv}{\int_S |\mathbf{B}|^2 ds}. \quad (60)$$

This formula is quite general, and in particular can also be used for a traditional cylindrical cavity of radius R_c and height h . In that case, the cylindrically symmetric $n = 0$ TM mode used for acceleration is given by

$$E_x(\rho, t) = \mathcal{N} J_0(k_0 \rho) \exp(-i\omega_0 t) \quad (61)$$

$$B_\varphi(\rho, t) = i\mathcal{N} J'_0(k_0 \rho) \exp(-i\omega_0 t) \quad (62)$$

where $k_0 = \omega_0/c$, J_0 is a Bessel function, and ρ and φ are cylindrical coordinates (cylindrical axis along x).

The vanishing of E_x on an ideally conducting cylindrical wall requires that $(\omega_0/c)R_c = 2.405$ (the smallest zero of J_0) which defines the angular resonant frequency in terms of R_c . Equations (62) and (60) lead to the well known formula for the quality of the cylindrical pill box cavity

$$Q_c = 2.405 \sqrt{\frac{2\pi\sigma}{\omega_0}} \frac{1}{1 + R_c/h}. \quad (63)$$

For the SLAC pill box cavity shown in **Figure 1** ($R_c = h = d = 4$ cm, and $\sigma = 5.294 \times 10^{17} \text{ s}^{-1}$ for copper wall in room-temperature), this formula leads to $Q_c = 1.633 \times 10^4$. The corresponding values for spherical cavities with ideal dielectric spheres and the same values of d and σ reach much larger values, see **Figure 11**.

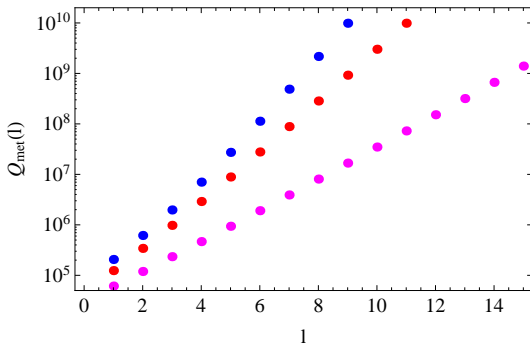


FIG. 11: The quality Q_{met} versus l for three spherical cavities with ideal dielectric spheres (see **Figure 6**).

In the presence of the dielectric sphere, one is also dealing with losses due to an imperfect dielectric specified by $\epsilon'' = \text{Im } \epsilon$. The non-vanishing value of ϵ'' leads to

$\text{Im } k \neq 0$, for k defined by (35). In view of Eq. (2) this implies a complex value of $\omega = \omega' + i\omega''$.

For the fields given by (4) – (9), we obtain

$$U(t) = U(t=0)e^{2\omega''t}$$

where $\omega'' < 0$ for the energy U being dissipated rather than generated. Using this result we find for the power losses in the dielectric:

$$P_{\text{diel}} = -\frac{dU}{dt} = -2\omega''U.$$

In view of (55), the corresponding quality will thus be given by

$$Q_{\text{diel}} = -\frac{\omega_0}{2\text{Im } \omega}. \quad (64)$$

This value is of the order of $(\tan \delta)^{-1} \equiv \epsilon'/\epsilon''$. It is approximately l independent.

In our calculations we took $\epsilon' = 10$ and $\epsilon'' = 10^{-6}$. Dielectrics with such ultra small losses were investigated in [8].

The total power loss in the spherical cavity encasing the dielectric sphere P_s is due to the power loss in the metallic wall and that in the dielectric sphere:

$$P_s = P_{\text{met}} + P_{\text{diel}}. \quad (65)$$

Dividing both sides of this relation by $\omega_0 U$ and using (55) we obtain

$$\frac{1}{Q_s} = \frac{1}{Q_{\text{met}}} + \frac{1}{Q_{\text{diel}}}. \quad (66)$$

where Q_s is the total Q-factor of the spherical cavity. Values of Q_s versus l for three spherical cavities with dielectric spheres and $d = 4$ cm are shown in **Figure 12**. They are about three orders of magnitude larger than $Q_c = 1.633 \times 10^4$.

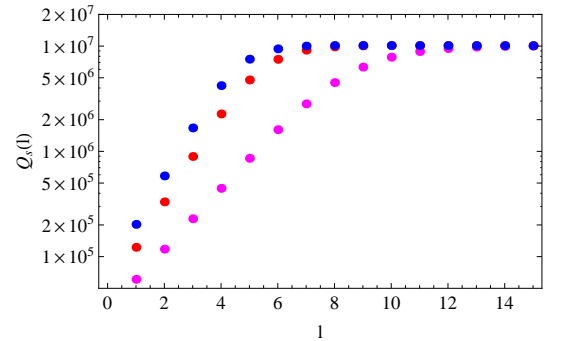


FIG. 12: The quality Q_s versus l for three spherical cavities with dielectric spheres (see **Figure 6**).

In a real accelerator, openings in the metallic wall are necessary for free penetration of the cavity by the electron beam, and to enable coupling between neighbouring cavities. This will lower the quality Q_{met} but should have

little effect on the total quality of the spherical cavity Q_s . The latter is defined by losses in the dielectric, see (66) where $Q_{\text{diel}} \ll Q_{\text{met}}$. The resonant frequency should not be drastically changed either, as the EM fields at the iris ($r = b$) are very small fractions of their maxima, see **Figure 4**.

C. Discussion and summary

When comparing the effective accelerating fields in the traditional pill box cavity with that in our spherical cavities with dielectric spheres, we first assume that U , the time-averaged energy stored in the cavity, see (56), is the same in both situations. Therefore the normalization factor \mathcal{N} in (61) and (62) will first be chosen so that

$$2\pi h \frac{1}{2} \int_0^{R_c} \rho d\rho [|E_x(\rho, t)|^2 + |B_\varphi(\rho, t)|^2] = 1 \quad (67)$$

see (42) ($U = 1/(8\pi)$ erg).

The complex effective accelerator field \bar{E} for the cylindrical resonator shown in **Figure 1** ($R_c = h = d$) is given by the right hand side of (45) in which E_x is defined by (61) with $\rho = 0$, and $\omega^l = \omega_0$. The result is

$$\bar{E}_c = \mathcal{N} \frac{\sin \alpha}{\alpha} e^{-i\omega_0 t_0}, \quad \alpha = \frac{\omega_0 d}{2c} \quad (68)$$

where t_0 is the time at which the electron passes the center of the cavity.

We now denote by E_{eff_s} and E_{eff_c} the maximal effective accelerating fields (equal to $|\bar{E}|$) for the spherical cavity with a dielectric sphere and the traditional cylindrical cavity, for any values of the average energies in the cavities, U_s and U_c . In view of the fact that E_x in (61) is proportional to \sqrt{U} we can write, using the definition (55) of Q ,

$$\frac{E_{\text{eff}_s}}{E_{\text{eff}_c}} = \sqrt{\frac{P_s}{P_c}} G(l) \quad (69)$$

where $G(l)$, the “gain factor”, is given by

$$G(l) = \frac{E_{\text{eff}_s}}{E_{\text{eff}_c}} \bigg|_{U_s=U_c} \sqrt{\frac{Q_s}{Q_c} \frac{\nu_c}{\nu_s}}. \quad (70)$$

Here ν_s and ν_c are the resonant frequencies of the spherical and the cylindrical cavities ($\nu = \omega_0/(2\pi)$) and P_s and P_c are the corresponding power losses. They are equal to the powers that must be supplied from external sources to sustain the oscillations. They should be as large as possible to avoid breakdown in the dielectric or at the metallic wall. Further research is necessary to give an estimate of the ratio P_s/P_c . We can only hope that it is not smaller than unity.

For our typical SLAC pill box cavity shown in **Figure 1** ($R_c = h = d = 4$ cm) we obtain $\nu_c = 2.87$ GHz and

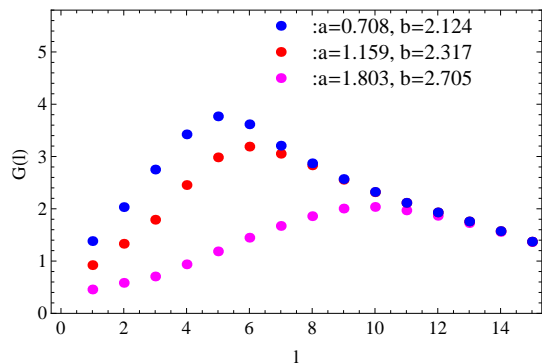


FIG. 13: Gain factor $G(l)$ in (69) and (70) for three spherical cavities (a and b in cm).

$E_{\text{eff}_c} |_{U_c=1/(8\pi) \text{ erg}} = 3.16$ kV/m, to be used in (70). The resulting values of the gain factor are shown in **Figure 13**.

The results of our calculation are shown in **Figures 3 – 13** for three reasonable values of $b/a = 3, 2, \frac{3}{2}$. The electron trajectory segment inside the cavity shown in **Figure 1** was equal to the typical length of the pill-box cavity of SLAC (4 cm). Calculations were performed for various values of l and m . The optimal parameters found were: $a = 0.708$ cm, $b = 2.124$ cm, and $(l, m) = (6, -2)$.

IV. CONCLUSIONS

An electric field, intensified by structural resonance, can be used to accelerate electrons. This is demonstrated here by placing a dielectric sphere concentrically inside a spherical resonator, in which an appropriate whispering gallery mode is excited. A strong, accelerating field appears next to the surface of the dielectric. At the same time, the tangential component of the magnetic field at the wall of the resonator is minimal. This makes losses at the metallic walls negligible without engaging expensive cryogenic systems ensuring superconductivity of the walls. The Q factor of the resonator only depends on losses in the dielectric. For existing dielectrics, this gives a Q factor three orders of magnitude better than obtained in existing cylindrical cavities. Furthermore, for the proposed spherical cavity, *all* field components at the metallic wall are either zero or very small, see **Figure 4**. Therefore, one can expect the proposed spherical cavity to be less prone to electrical breakdowns than the traditional cylindrical cavity.

Acknowledgments

The authors would like to thank Professor Stanisław Kuliński for useful discussions.

-
- [1] W. Żakowicz, “Whispering-Gallery-Mode Resonances: A New Way to Accelerate Charged Particles,” *Physical Review Letters*, Vol. 95, 2005, pp. 114801-114804. doi:10.1103/PhysRevLett.95.114801
 - [2] W. Żakowicz, “Erratum: Whispering-Gallery-Mode Resonances: A New Way to Accelerate Charged Particles [Phys. Rev. Lett. 95, 114801 (2005)],” *Physical Review Letters*, Vol. 97, 2006, p. 109901. doi:10.1103/PhysRevLett.97.109901
 - [3] W. Żakowicz, “Particle acceleration by wave scattering off dielectric spheres at whispering-gallery-mode resonance,” *Physical Review Special Topics—Accelerators and Beams*, Vol. 10, 2007, pp. 101301-101309. doi:10.1103/PhysRevSTAB.10.101301
 - [4] M. Ornigotti and A. Aiello, “Theory of anisotropic whispering-gallery-mode resonators,” *Physical Review A*, Vol. 84, 2011, pp. 013828-013839. doi:10.1103/PhysRevA.84.013828
 - [5] T. V. Liseykina, S. Pirner and D. Bauer, “Relativistic Attosecond Electron Bunches from Laser-Illuminated Droplets,” *Physical Review Letters*, Vol. 104, 2010, pp. 095002-095005. doi:10.1103/PhysRevLett.104.095002
 - [6] V. S. Ilchenko, A. A. Savchenkov, A. B. Matsko and L. Maleki, “Nonlinear Optics and Crystalline Whispering Gallery Mode Cavities,” *Physical Review Letters*, Vol. 92, 2004, pp. 043903-043906. doi:10.1103/PhysRevLett.92.043903
 - [7] R. C. Taber and C. A. Flory, “Microwave oscillators incorporating cryogenic sapphire dielectric resonators,” *IEEE Transactions on Ultrasonics, Ferroelectrics and Frequency Control*, Vol. 42, 1995, pp. 111-119. doi:10.1109/58.368306
 - [8] J. Krupka, K. Derzakowski, M. E Tobar, J. Hartnett, and R. G. Geyer, “Complex permittivity of some ultralow loss dielectric crystals at cryogenic temperatures,” *Measurement Science and Technology*, Vol. 10, 1999, pp. 387-392. doi:10.1088/0957-0233/10/5/308
 - [9] J. D. Jackson, “Classical electrodynamics,” 3rd ed., John Wiley, New York, 1998.
 - [10] A. Moroz, “A recursive transfer-matrix solution for a dipole radiating inside and outside a stratified sphere,” *Annals of Physics*, Vol. 315, 2005, pp. 352-418. doi:10.1016/j.aop.2004.07.002